Checkerboard patterns of charge stripes in the two-gap superconductor ZrB_{12}

N. B. Bolotina ⓘ,[1] O. N. Khrykina ⓘ,[1] A. N. Azarevich ⓘ,[2] N. Yu. Shitsevalova ⓘ,[3] V. B. Filipov,[3] S. Yu. Gavrilkin,[4]
K. V. Mitsen,[4] V. V. Voronov,[2] and N. E. Sluchanko ⓘ[2]

[1]*Shubnikov Institute of Crystallography, Federal Scientific Research Centre "Crystallography and Photonics" of
Russian Academy of Sciences, Leninskiy Avenue 59, 119333 Moscow, Russia*
[2]*Prokhorov General Physics Institute of Russian Academy of Sciences, Vavilov Street 38, 119991 Moscow, Russia*
[3]*Frantsevich Institute for Problems of Materials Science, National Academy of Sciences of Ukraine, 03680 Kyiv, Ukraine*
[4]*Lebedev Physical Institute of Russian Academy of Sciences, Leninskiy Avenue 53, 119991 Moscow, Russia*

Inhomogeneous superconductivity was studied in ZrB_{12} ($T_c \approx 6$ K) using heat capacity and x-ray diffraction data. Evidence of two-band superconductivity with two branches of upper critical field $\mathbf{H}_{c2}(T_c)$ is obtained in a magnetic field applied along the [110] axis of the crystal. On the contrary, at $\mathbf{H} \parallel [100]$, a single dependence $\mathbf{H}c_2(T_c)$ was observed. This finding is consistent with the checkerboard-type patterns observed on the difference Fourier maps of the electron density distribution. These patterns are compared to those for the weakly coupled superconductor LuB_{12}, T_c of which is 15 times lower than that of ZrB_{12}. The probable nature of the two-gap superconductivity in ZrB_{12} is discussed.

I. INTRODUCTION

In the study of high-temperature superconductivity (HTSC) in conventional (MgB_2 [1]) and unconventional (cuprates, Fe-based pnictides and chalcogenides [2–6]) superconductors, many unusual phenomena were discovered, including charge and spin stripes [2–4], electron nematic effects [2], and multiband superconductivity of various types [5–7]. It is assumed that at least some of these features are closely related to the mechanisms of the superconductivity enhancement [2–7]; therefore, the elucidation of the nature of these anomalies and their relationship with HTSC is extremely important. It is currently believed that a simultaneous activity of the charge, spin, lattice, and orbital interactions plays a key role in the formation of complex phase diagrams of these superconductors and provides the main components of HTSC [2–8].

The microscopic mechanism that causes a material to form charge stripes due to the interaction of charge and lattice degrees of freedom was recently elucidated for the weakly coupled superconductor LuB_{12} ($T_c \approx 0.42$ K). According to [9,10], cooperative Jahn-Teller (JT) instability (ferrodistortive effect) of the rigid boron framework is a factor responsible for periodic changes in the $5d$-$2p$ hybridization of the conduction-band states, which leads to the formation of *dynamic charge stripes* in the fcc lattice of LuB_{12} along directions $\langle 110 \rangle$. As shown in [11] for $Lu_xZr_{1-x}B_{12}$ solid solutions, charge fluctuations at the Lu sites cause a pair-breaking effect, which leads to a 15-fold decrease in T_c with increasing x. ZrB_{12} is a two-gap strongly coupled superconductor with $T_c \approx 6$ K (see [11] and references therein), but the possible reasons for the increase in T_c and variations in the electron-phonon interaction $\lambda_{e\text{-ph}}$ in the range 0.4–1 are not yet clear. Taking

into account that a large pseudogap ($\Delta_{ps\text{-gap}} \approx 7.3$ meV) was detected by high-resolution photoemission spectroscopy in ZrB_{12} above T_c, and the proximity to the quantum fluctuation regime was predicted from *ab initio* calculations of the band structure [12], a detailed study of the crystal and electronic structure as well as the anisotropy of the superconducting state in the two-gap superconductor ZrB_{12} seem promising in the search for regularities that can be important for HTSC.

The crystal structure of ZrB_{12} is studied in this work at room and low temperatures. Small static Jahn-Teller distortions of the fcc lattice are observed. The detected charge stripes form two grids from rhomboid cells (*checkerboard patterns*) built from (i) hybridized $4d$-$2p$ and (ii) only $2p$ conduction-band states. The characteristics of the two-gap superconductivity are confirmed by measurements of the low-temperature heat capacity. We conclude in favor of magnetic-field-induced anisotropy, which arises from the interaction between vortices and a two-band filamentary structure with fluctuating electron density (charge stripes).

II. EXPERIMENT

The high-quality single crystals of ZrB_{12} were cut from the same rods as in [11]. A Bruker D8 Discover x-ray diffractometer was used to control the quality of initial crystal disks with a diameter of about 6 mm and a thickness of 1 mm (see Sec. 1 of the Supplemental Material [13] for more details). The heat capacity measurements on square samples $\sim 2 \times 2 \times 0.5$ mm³ in size were carried out on PPMS-9 (Quantum Design).

Spherical samples of about 0.3 mm in diameter were prepared for x-ray data collection (see [9,14] for more details). The x-ray data sets (Mo $K\alpha$ radiation, $\lambda = 0.7093$ Å) were

obtained at 97 K and at room temperature 293 K on an Xcalibur diffractometer (Oxford Diffraction). To cool the sample, a Cobra Plus cryosystem (Oxford Cryosystems) was applied with an open stream of cold nitrogen directed at the sample. The crystal structure of ZrB_{12} was refined in the $Fm\bar{3}m$ group using the JANA2006 program [15]. The unit cell of the fcc lattice contains two symmetrically independent atoms: Zr in the fixed position 4a (0, 0, 0) and B in the special position 48i (1/2, y, y), $y \approx 1/6$. Each Zr atom is surrounded by 24 boron atoms and 12 Zr atoms, $d(\text{Zr–Zr}) = a_{\text{cub}}/\sqrt{2} \approx 5.23$ Å. Other details of the data collection and structure refinement are summarized in Tables S1 and S2 of the Supplemental Material [13].

III. RESULTS

A. Crystal and electron structure

The crystal structure of ZrB_{12}, typical for most dodecaborides, is schematically presented in Fig. 1(a). As shown in [16], charge transfer across the bridge between two Zr atoms is possible through a pair of boron atoms owing to significant overlapping at the Fermi level (E_F) between the B–B π-bond and 4d orbital of Zr. Charge transfer along the Zr-B-B-Zr bridges is possible in six directions $\langle 110 \rangle$, which are equivalent in a cubic structure. The plane (111) in Fig. 1(b) contains three such directions indicated by dashed lines. Boron atoms forming three B-B pairs go out of the plane by ± 0.8 Å. Three atoms, one from each pair, form a triangular face of the B_{12} cubooctahedron, while the other three belong to three different cubooctahedra.

The geometry of the negatively charged clusters $[B_{12}]^{n-}$ was earlier [10,17] optimized within the framework of density functional theory (DFT), which made it possible to conclude in favor of their JT distortions (see Sec. 2 in the Supplemental Material [13]). The result of DFT calculations for the cluster $[B_{12}]^{2-}$, which is the element of ZrB_{12} crystal structure, is shown in Fig. 1(c). Parallel alignment of local distortions of B_{12} cubooctahedra (known as the *ferrodistortive* case) can lead to static and dynamic JT deformations of the fcc lattice as a whole. When the lattice parameters of ZrB_{12} were refined without imposing symmetry bonds, the very small but well-detected static JT distortions of the cubic lattice were found at both 293 and 97 K (less than 0.005 Å in length and 0.03° in angles; see Table I).

With such minor violations, it makes no sense to lower the symmetry of the structural model; all our attempts to do this were ineffective. At the same time, the *static lattice distortions* are a fingerprint of the *dynamic JT instability* [10,18]. This leads to an asymmetric redistribution of electrons along the directions of metal-boron and boron-boron bonds in the interstices of the crystal lattice. Their visualization on the Fourier maps of the difference electron density $\Delta\rho(\mathbf{r})$ is provided in a simple, although unusual, way for traditional structural analysis. As is known, $\Delta\rho(\mathbf{r})$ can be calculated at any point of the unit cell by the following formula:

$$\Delta\rho(\mathbf{r}) = \frac{1}{V} {}^* \sum_{\mathbf{H}} [|F_{\text{obs}}(\mathbf{H}) - F_{\text{calc}}(\mathbf{H})|]\exp[-2\pi i(\mathbf{r} \cdot \mathbf{H})].$$
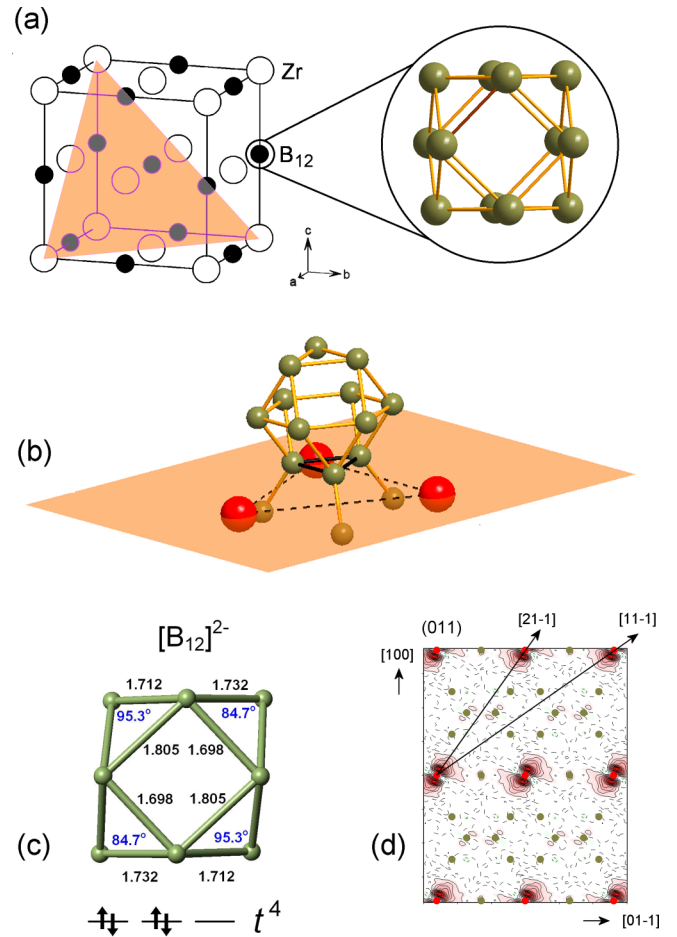

FIG. 1. (a) Schematic representation of the NaCl-type unit cell of ZrB_{12}. Open circles are Zr atoms, dark circles are B_{12} cubooctahedra, one of which is shown on the right. The (111) plane is highlighted. (b) Three Zr atoms (large red balls) and six boron atoms [small balls, orange below and khaki above the (111) plane] form three Zr-B-B-Zr bridges. (c) Theoretical JT distortions of a negatively charged $[B_{12}]^{-2}$ cluster. (d) Difference Fourier synthesis of electron density (ED) in the (011) plane at $T = 97$ K. Red circles are Zr sites in the plane; khaki circles are boron sites at distances less than 1 Å from the plane. Positive ED residues are shown in shades of red. Contour interval is $0.5\,e/\text{Å}^3$.

Here V is a unit-cell volume; $\mathbf{H} = \mathbf{H}(hkl) = \mathbf{S}-\mathbf{S}_0$, where $\mathbf{S}_0$ and $\mathbf{S}$ are direct and diffracted x-ray beams, respectively, and $F_{\text{obs}}(\mathbf{H}) - F_{\text{calc}}(\mathbf{H})$ is the difference between the modules of the observed (measured) and calculated structural factors. As one can see, this formula does not contain any information on the crystal symmetry. Structural factors $F_{\text{calc}}(\mathbf{H})$ are calculated from the structural parameters refined in the $Fm\bar{3}m$ group. Traditionally, synthesis is carried out in a symmetrically independent volume of a unit cell, and the result is extended to the entire cell using symmetry operators. In other words, the symmetry of the difference Fourier maps exactly corresponds to the space group supplied to the input of the synthesis procedure. Even if the violations do occur, they will not appear on the maps. Our departure from tradition concerns $|F_{\text{obs}}(\mathbf{H})|$, which in this case are not averaged in the Laue class $m\bar{3}m$, and the difference Fourier synthesis is not

TABLE I. The unit-cell parameters of ZrB$_{12}$, determined from x-ray data obtained with (a_{cub}) and without (a, b, c, α, β, γ) imposing symmetry bonds.

T (K)	a_{cub} (Å)	a (Å)	b (Å)	c (Å)	α (deg)	β (deg)	γ (deg)
293	7.40203(2)	7.4045(1)	7.4035(1)	7.3981(1)	89.988(1)	90.024(1)	90.021(1)
97	7.39854(3)	7.4003(1)	7.3981(1)	7.3972(1)	90.010(1)	90.033(1)	90.007(1)

limited to a small unit-cell volume, independent in the $Fm\bar{3}m$ group.

Such an approach was previously applied to other JT-active dodecaborides LuB$_{12}$ [9,10] and (Tm, Yb)B$_{12}$ [10,14]. In ZrB$_{12}$, positive residuals of electron density near Zr sites form a flat, highly anisotropic butterfly-shaped figure with wings parallel to the (011) plane [Fig. 1(d)]. If interatomic distances are calculated from the lattice parameters distorted by the JT effect, cuboctahedra B$_{12}$ are slightly elongated along [11-1] and compressed in the perpendicular plane (11-1), as was theoretically predicted [Fig. 1(c)] for the ferrodistortive JT state [10,17]. At room temperature, this effect is partially suppressed by the thermal motion of the atoms.

The advantageous charge transfer along [01-1] across the Zr-B-B-Zr bridge is evident in the plane (011) from Fig. 1(d). In the (111) plane [Fig. 2(a)], one more direction is distinguished in addition to [01-1], namely, [1-10]. As follows from Fig. 2(b), charge transfer in the (11-1) plane along Zr-B-B-Zr bridges is less probable, but excess electrons are collected between the boron sites, mainly along [011] and [1-10] directions.

The results allow us to (i) conclude that these (111) and (11-1) planes become not equivalent in the JT-active fcc lattice and (ii) make an assumption about the ways of charge transfer in ZrB$_{12}$. The conclusion by Ma *et al.* [16] on the formation of Zr-B-B-Zr bridges along the ⟨110⟩ directions owing to overlapping at the Fermi level between the B-B π bond and $4d$ orbital of Zr should be supplemented with the assumption of additional charge transfer over the boron states bypassing $4d$ orbitals of zirconium.

Fine electron structure of LuB$_{12}$, previously studied in a similar way [9], demonstrated the only linear charge stripes running through the Lu-B-B-Lu bridges in this superconductor with $T_c \approx 0.42$ K.

B. Two-gap superconductivity in ZrB$_{12}$

The temperature dependencies of the heat capacity $C(T, H_0)$ of ZrB$_{12}$ single crystals were recorded in the temperature range 0.4–7 K in magnetic fields up to 3 kOe applied along the [100] [Fig. 3(a)] and [110] [Fig. 3(b)] directions. They contain one stepped singularity for **H** ∥ [100], but for **H** ∥ [110], two adjacent humps (the main and the smaller one) can be distinguished, which correspond to superconducting transitions. Finer details can be seen in the temperature dependencies of the derivatives $dC/dT = f(T, H_0)$ presented in Sec. 4 of the Supplemental Material [13]. Figure 3(c) contains temperature dependencies of thermodynamic $H_{\text{cm}}(T)$ and upper $H_{c2}(T)$, $H'_{c2}(T)$ critical fields (see Secs. 3 and 4 in the Supplemental Material [13] for more details). The normalized heat capacity curve at zero field, $C/\gamma T = f(T/T_c)$, in the superconducting state is shown in Fig. 3(d). It is interesting to note that in the 4–6 K temperature range [Fig. 3(c)], the smaller-gap superconductivity for **H** ∥ [110] belongs to type I, but at $T^* \sim 4$ K, a transition from type I to type II is observed in the lower band. On the contrary, for **H** ∥ [100], only one $H_{c2}(T)$ branch is observed, demonstrating type II one-band behavior. Moreover, below $T^* \sim 4$ K a significant discrepancy appears between the upper band $H'_{c2}{}^{[110]}(T)$ and $H_{c2}{}^{[100]}(T)$, revealing an unusual dependence of the upper
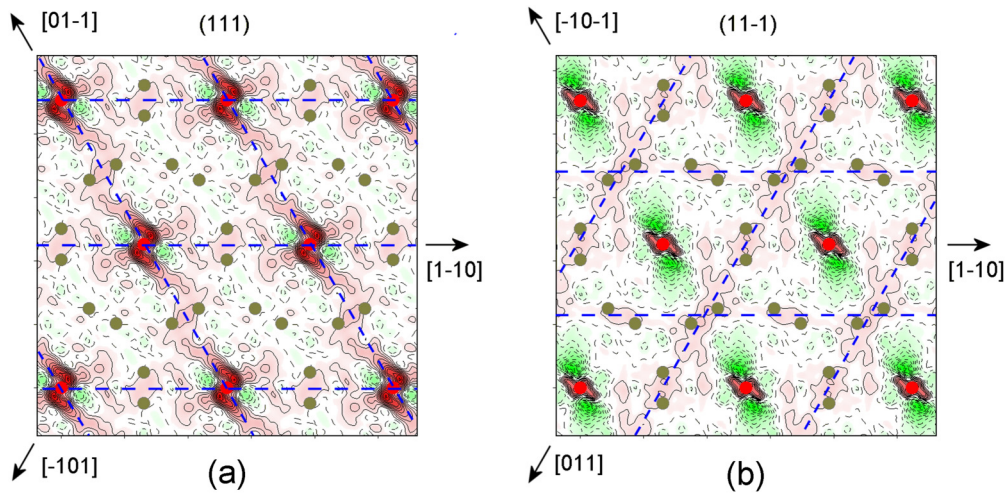

FIG. 2. Distribution of difference electron density in a 12×12 Å fragment of (a) (111) and (b) (11-1) plane of the ZrB$_{12}$ crystal lattice at $T = 97$ K. Red circles are Zr sites in the plane; khaki circles are boron sites at distances less than 1 Å from the plane. Positive and negative ED residues are shown in shades of red and green, respectively. Contour intervals are $0.2\,e/$Å^3; (a) $\Delta\rho(\text{max})/\Delta\rho(\text{min}) = 2.4/-1.2\,e/$Å^3 and (b) $1.9/-2.5\,e/$Å^3 (b). The dotted blue lines are guides for the eye demonstrating the stripe configurations in the planes.
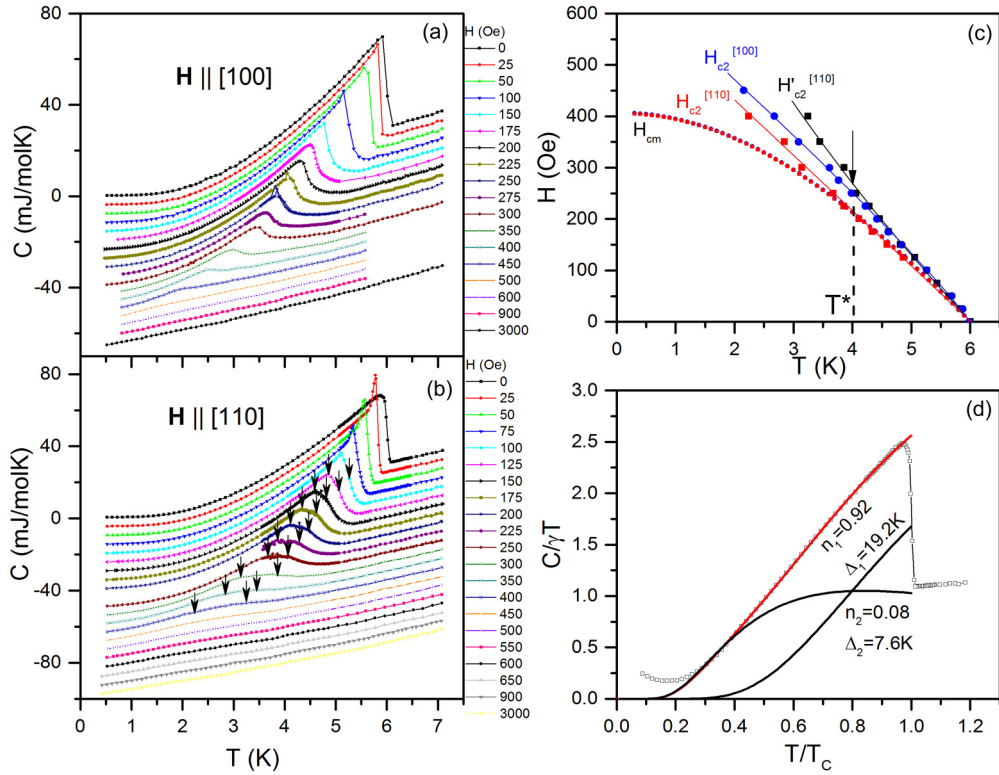
FIG. 3. Temperature dependencies of the heat capacity $C(T, H_0)$ of ZrB$_{12}$ single crystals in magnetic fields $H_0 \leqslant 3$ kOe applied along (a) [100] and (b) [110] directions (curves are vertically shifted for clarity). Arrows in panel (b) mark two adjacent transitions. (c) Thermodynamic $H_{cm}(T)$ and upper $H_{c2}(T)$, $H'_{c2}(T)$ critical fields for **H** ∥ [100] and **H** ∥ [110], and (d) the zero-field normalized heat capacity $C/\gamma T = f(T/T_c)$ in the superconducting state [see text and Eq. (5.3) in the Supplemental Material [13] for more details]. The arrow in panel (c) denotes the transition at $T^* \sim 4$ K inside the superconducting state.

critical field on the direction of the external magnetic field. Thus, the anisotropy $H_{c2}(T)$ appears slightly below $T^* \sim 4$ K and increases with decreasing temperature. Finally, it should be noted in this section that a similar phase transition was observed at $T^* = 4.2$–4.7 K in the superconducting state of Zr^{N}B$_{12}$ crystals with different boron isotopes ($N = 10, 11$, and nat) [19].

IV. DISCUSSION

First of all, note that two-band superconductivity was definitely detected in the recent μSR experiments, which were carried out in both Lu$_x$Zr$_{1-x}$B$_{12}$ [20] and ZrB$_{12}$ [21], and was also established in previous heat capacity measurements [11]. In addition, a sharp peak in the heat capacity of ZrB$_{12}$ [see Fig. 3(b), $H < 100$ Oe] was detected earlier [22] in weak magnetic fields, and the singularities were attributed to the "type I - type II/1" transition predicted in the one-band model [23]. Considering that the single-band approach is not applicable to ZrB$_{12}$, a more correct description can be proposed in the two-band Lu$_x$Zr$_{1-x}$B$_{12}$ systems using the two-band Eilenberger formalism (see, for example [24,25]). According to [24] (see also the recent calculation for ZrB$_{12}$ in [21]), in the case of a two-band superconductor of type 1.5 in low magnetic fields, a transition to an additional semi-Meissner phase is observed, which is a macroscopic phase separation into (i) domains of a two-component vortex state and (ii) vortex clusters in which one of the components is suppressed.

To summarize, we can say that there are several features of type 1.5 superconductivity: (i) Meissner state in low fields, (ii) macroscopic phase separation into vortex clusters coexisting with Meissner domains in intermediate fields (semi-Meissner phase), and (iii) vortex lattices and/or liquids in larger fields. Vortices are formed as a result of a first-order phase transition. The transition from the vortex states to the normal state is a second-order phase transition. Moreover, in ZrB$_{12}$, which is a two-gap superconductor with dynamic charge stripes, the interaction of these fluctuating charges (high-frequency alternating current $\sim$200 GHz, which is quantum in nature; see [14] for more details) with vortices is possible even in low magnetic fields, inducting strong anisotropy of superconducting characteristics.

The zero-temperature critical fields $H_{cm}(0)$, $H_{c2}^{[110]}(0)$, $H_{c2}'^{[110]}(0)$, and $H_{c2}^{[100]}(0)$ derived in this study allow us to estimate the coherence length of the upper band $\xi_1(0) \approx$ 739 Å (see Sec. 3 in the Supplemental Material [13] for more details). Indeed, according to [24,25], the true H_{c2} gives an accurate shorter coherence length, but the longer one ($\approx$766 Å) is obviously underestimated for two reasons:

(1) As the field decreases, nonlinear terms and interband coupling become important, which leads to the nucleation of a substantial density of the second mode in higher fields than predicted by the standard theory of type-II superconductivity.

(2) The second H_{c2}-like feature is observed when the dominant component already contributes to the screening of the field; therefore, the second component can be nucleated with

a much larger coherence length than predicted by the standard single-band theory.

In view of the above, the longer coherence length should be estimated by the inequality $\xi_2(0) > 766$ Å. Moreover, taking from [20] [see Fig. 2(h) there] an estimate of the penetration depth $\lambda(ZrB_{12}) \sim 1800$ Å, the inequality $\xi_2(0) \geqslant 2000$ Å can be naturally proposed for the lower band in the case of two-band s-wave type-1.5 superconductivity.

Thus, the correlation lengths of the upper band, $\xi_1(0) \approx 739$ Å, and the lower band, $\xi_2(0) \geqslant 2000$ Å, differ greatly. We also note that the value of the penetration depth and the coherence length $\xi(LuB_{12}) \sim 4000$ Å, estimated in [11], agree with the type-I superconductivity found for LuB_{12}.

When fitting the two-band α model (Sec. 4 in the Supplemental Material [13]), the gap energies $\Delta_1(0)/k_B \approx 19.2$ K and $\Delta_2(0)/k_B \approx 7.6$ K were calculated in combination with the relative weight $n_2(x) \approx 0.08$ of the small-gap component. The ratios $2\Delta_1(0)/k_B T_c \approx 6$ and $2\Delta_2(0)/k_B T_c \approx 2.5$ obtained here are evidence in favor of superconductivity with strong and weak coupling in the upper and lower bands, respectively.

Calculations of the band structure in the rigid fcc lattice of ZrB_{12} [12,26,27] predict only hybridized states of the $4d$-$2p$ conduction band near E_F. On the contrary, static and dynamic JT distortions observed in ZrB_{12} give rise to another conduction band constructed from $2p$ boron orbitals. It can be assumed that two-band superconductivity is characteristic of two-band metallic ZrB_{12}. Its conducting channels form two filamentary structures in the crystal, each in the form of a grid with rhomboid cells (a checkerboard pattern). One of them is generated by hybridized $4d$-$2p$ orbitals, while the other is generated by the states of the $2p$ conduction band. Note that the arrangement of the two types of plane grids of stripes can be considered as a factor responsible for the field-induced anisotropy of superconductivity detected in the study of heat capacity [Fig. 3(c)]. The situation is actually much more complicated than in the case of a "simple" two-band s-wave superconductor of type 1.5, due to the presence of spatially oriented dynamic charge stripes that strongly interact with vortices. As a result, the vortex structure in ZrB_{12} becomes strongly dependent on the orientation and strength of the external magnetic field, which leads to an anisotropic phase diagram with a number of superconducting phases and phase transitions between them.

When comparing the conduction band of dodecaborides LuB_{12} and ZrB_{12}, which have a similar fcc structure and similar phonon spectra, one should take into account the difference in the valences of Zr (4+) and Lu (3+). The only one $5d$ electron of the Lu^{3+} ion participates in the formation of $5d$-$2p$ hybridized conduction states, with the charge stripes located along the $\langle 110 \rangle$ directions in the fcc lattice [9,10]. To the contrary, each Zr^{4+} ion in ZrB_{12} gives two $4d$ electrons, which contribute to the conduction states. This leads both to an increase in E_F by about 0.3-0.4 eV [27] and to the appearance of two checkerboard patterns in the filamentary structure of the conduction channels (Fig. 2). According to the conclusions [2-4], charge stripes should be considered as important components of HTSC. Moreover, in [28], a new scenario was proposed based on the formation of pair density waves (PDWs) and charge density waves (CDWs), which underlie the emergence of a complex inhomogeneous superconducting state in the HTSC. This kind of PDW, which intertwines both CDWs and superconducting orders, can also be proposed to explain inhomogeneous superconductivity using the checkerboard patterns of charge stripes observed in ZrB_{12}.

V. CONCLUSION

Precise x-ray diffraction measurements of high-quality ZrB_{12} crystals and the data analysis undertaken here establish both the static Jahn-Teller distortions of the fcc lattice and appearance of two types of checkerboard patterns of the dynamic charge stripes in this inhomogeneous superconductor. Our results of studying the low-temperature heat capacity allow us to conclude in favor of two-gap superconductivity and a noticeable anisotropy of the upper critical field H_{c2} $H_{c2}(T_c)$, which also depends on the orientation of the magnetic field vector. The estimates of the coherence lengths $\xi_1(0) \approx 739$ Å and $\xi_2(0) \geqslant 2000$ Å, the energy gaps $\Delta_1(0)/k_B \approx 19.2$ K and $\Delta_2(0)/k_B \approx 7.6$ K, and ratios $2\Delta_1(0)/k_B T_c \approx 6$ and $2\Delta_2(0)/k_B T_c \approx 2.5$ characterize superconductivity in the upper strongly coupled and lower weakly coupled bands, respectively. We propose that the spatially modulated superconducting order in ZrB_{12} could be discussed in terms of the PDW scenario developed recently for HTSC [28].

[1] J. Nagamatsu, N. Nakagawa, T. Muranaka, Y. Zenitani, and J. Akimitsu, Nature (London) **410**, 63 (2001).

[2] B. Keimer, S. A. Kivelson, M. R. Norman, S. Uchida, and J. Zaanen, Nature (London) **518**, 179 (2015).

[3] E. Berg, E. Fradkin, S. A. Kivelson, and J. M. Tranquada, New J. Phys. **11**, 115004 (2009).

[4] S. Sachdev and B. Keimer, Phys. Today **64**(2), 29 (2011).

[5] P. J. Hirschfeld, M. M. Korshunov, and I. I. Mazin, Rep. Prog. Phys. **74**, 124508 (2011).

[6] G. R. Stewart, Rev. Mod. Phys. **83**, 1589 (2011).

[7] M. Zehetmayer, Supercond. Sci. Technol. **26**, 043001 (2013).

[8] E. Dagotto, Science **309**, 257 (2005).

[9] N. B. Bolotina, A. P. Dudka, O. N. Khrykina, V. N. Krasnorussky, N. Y. Shitsevalova, V. B. Filipov, and N. E. Sluchanko, J. Phys. Condens. Matter **30**, 265402 (2018).

[10] N. B. Bolotina, A. P. Dudka, O. N. Khrykina, and V. S. Mironov, Crystal structure of dodecaborides: Complexity in simplicity, in *Rare-Earth Borides*, edited by D. S. Inosov (Jenny Stanford Publishing, Singapore, 2021), Chap. 3, pp. 293–330.

[11] A. Azarevich, A. Bogach, V. Glushkov, S. Demishev, A. Khoroshilov, K. Krasikov, V. Voronov, N. Shitsevalova, V. Filipov, S. Gabáni, K. Flachbart, A. Kuznetsov, S. Gavrilkin, K. Mitsen, S. J. Blundell, and N. E. Sluchanko, Phys. Rev. B **103**, 104515 (2021).

[12] S. Thakur, D. Biswas, N. Sahadev, P. K. Biswas, G. Balakrishnan, and K. Maiti, Sci. Rep. **3**, 3342 (2013).

[13] See Supplemental Material at http://link.aps.org/supplemental/10.1103/PhysRevB.105.054511 for Experimental details and refinement parameters for the ZrB_{12} crystal structure (Tables S1 and S2), orientation and quality control of single-domain crystals (Figs. S1–S3), DFT calculations (Fig. S4), estimations of thermodynamic and upper critical fields and superconductive state characteristics, derivatives $dC/dT = f(T, H_0)$ (Fig. S5).

[14] N. E. Sluchanko, A. N. Azarevich, A. V. Bogach, N. B. Bolotina, V. V. Glushkov, S. V. Demishev, A. P. Dudka, O. N. Khrykina, V. B. Filipov, N. Yu. Shitsevalova, G. A. Komandin, A. V. Muratov, Yu. A. Aleshchenko, E. S. Zhukova, and B. P. Gorshunov, J. Phys.: Condens. Matter **31**, 065604 (2019).

[15] V. Petříček, M. Dušek, and L. Palatinus, Z. Kristallogr. **229**, 345 (2014).

[16] H. Ma, T. Li. X. Zheng, Sh. Wang, X. Wang, H. Zhao, S. Han, J. Liu, R. Zhang, P. Zhu, Y. Long, J. Cheng, Y. Ma, Yu. Zhao, Ch. Jin, and Xiaohui Yu, Adv. Mater. **29**, 1604003 (2017).

[17] N. Sluchanko, A. Bogach, N. Bolotina, V. Glushkov, S. Demishev, A. Dudka, V. Krasnorussky, O. Khrykina, K. Krasikov, V. Mironov, V. B. Filipov, and N. Shitsevalova, Phys. Rev. B **97**, 035150 (2018).

[18] N. E. Sluchanko, Magnetism, quantum criticality, and metal-insulator transitions in RB_{12}, in *Rare-Earth Borides*, edited by D. S. Inosov (Jenny Stanford Publishing, Singapore, 2021), Chap. 4, pp. 331–442.

[19] N. E. Sluchanko, A. N. Azarevich, A. V. Bogach, S. Y. Gavrilkin, V. V. Glushkov, S. V. Demishev, A. V. Dukhnenko, A. B. Lyashchenko, K. V. Mitsen, and V. B. Filipov, JETP Lett. **94**, 642 (2011).

[20] F. K. K. Kirschner, N. E. Sluchanko, V. B. Filipov, F. L. Pratt, C. Baines, N. Yu. Shitsevalova, and S. J. Blundell, Phys. Rev. B **98**, 094505 (2018).

[21] P. K. Biswas, F. N. Rybakov, R. P. Singh, S. Mukherjee, N. Parzyk, G. Balakrishnan, M. R. Lees, C. D. Dewhurst, E. Babaev, A. D. Hillier, and D. Mc K. Paul, Phys. Rev. B **102**, 144523 (2020).

[22] Y. Wang, R. Lortz, Yu. Paderno, V. Filippov, S. Abe, U. Tutsch, and A. Junod, Phys. Rev. B **72**, 024548 (2005).

[23] G. Eilenberger, Phys. Rev. **153**, 584 (1967).

[24] M. Silaev and E. Babaev, Phys. Rev. B **84**, 094515 (2011).

[25] E. Babaev, J. Carlström, M. Silaev, and J. M. Speight, Type-1.5 superconductivity, in *Superconductors at the Nanoscale*, edited by R. Wördenweber, V. Moshchalkov, S. Bending, and F. Tafuri (De Gruyter, Berlin, Germany, 2017), Chap. 4, pp. 133–164.

[26] B. Jäger, S. Paluch, O. J. Zogał, W. Wolf, P. Herzig, V. B. Filippov, N. Shitsevalova, and Y. Paderno, J. Phys.: Condens. Matter **18**, 2525 (2006).

[27] J. Teyssier, R. Lortz, A. Petrovic, D. van der Marel, V. Filippov, and N. Shitsevalova, Phys. Rev. B **78**, 134504 (2008).

[28] E. Fradkin, S. A. Kivelson, and J. M. Tranquada, Rev. Mod. Phys. **87**, 457 (2015).